

Bayesian spatial+: A joint model perspective

Isa Marques^{*1} and Paul F.V. Wiemann¹

¹Department of Statistics, The Ohio State University, Columbus, OH, USA

Spatial confounding is a common issue in spatial regression models, occurring when spatially varying covariates correlate with the spatial effect included in the model. This dependence, particularly at high spatial frequencies, can introduce bias in regression coefficient estimates when combined with smoothing penalties. The spatial+ framework is a widely used two-stage frequentist approach that mitigates spatial confounding by explicitly modeling and removing the spatial structure in the confounding covariate, then using the corresponding residuals in the second-stage model for the response. However, it does not propagate first-stage uncertainty, does not discuss a general inferential framework, and, crucially, cannot guarantee that covariate residuals and spatial effects in the response model are free of shared high-frequency structure, so confounding may persist. We propose Bayesian spatial+, a joint modeling approach that simultaneously addresses these limitations. Our framework naturally propagates uncertainty and enables straightforward posterior inference, while ensuring separation of spatial frequencies through specialized joint priors on smoothness parameters. We further introduce a cut-feedback strategy that prevents feedback between model components from reintroducing confounding. Simulation studies and real-world applications show substantial gains in bias reduction and interval coverage relative to existing approaches. Notably, in our comparisons, Bayesian spatial+ is the only method for which credible interval coverage remains stable as the sample size increases.

1 Introduction

Spatial regression models are commonly employed to account for residual spatial dependence in a regression model after considering observed covariates. This residual spatial dependence can be thought of as the result of unobserved, spatially varying covariates. When these unobserved covariates are correlated with the observed covariates, the resulting regression coefficients may be biased, and their uncertainty underestimated.

A standard approach to adjust for unobserved spatial covariates is to approximate their collective effect using an unknown function f , defined over the spatial domain.

^{*}Corresponding author.

Consider observations $y(\mathbf{s}_i)$ within the spatial domain \mathcal{S} at locations $\mathbf{s}_i \in \mathcal{S} \subseteq \mathbb{R}^2$, for $i = 1, \dots, n$. These observations can be modeled as

$$y(\mathbf{s}_i) = x(\mathbf{s}_i)\beta + f(\mathbf{s}_i) + \varepsilon(\mathbf{s}_i),$$

where $x(\mathbf{s}_i)$ is a spatially-varying covariate, β is the associated coefficient, and each $\varepsilon(\mathbf{s}_i)$ is i.i.d. normally distributed with mean zero and constant variance. Throughout, we assume that covariates and response are centered at zero, such that intercepts can be omitted.

Unfortunately, spatial dependence between observed and unobserved covariates is often reflected in the spatial dependence between f and x . This correlation may lead to biased estimates of regression coefficients and inflated standard errors. This phenomenon, first identified by Clayton et al. (1993) and later termed “spatial confounding” by Reich et al. (2006), has been extensively studied, with numerous articles addressing its causes and mitigation strategies (e.g. Reich et al., 2006; Paciorek, 2010; Thaden and Kneib, 2018; Khan and Calder, 2020; Dupont et al., 2022; Marques et al., 2022; Guan et al., 2022; Dupont et al., 2023).

Recent advances have identified two key mechanisms driving spatial confounding: smoothing and spatial frequencies. Spatial confounding vanishes when no smoothing is applied to the spatial effect (Dupont et al., 2022, 2023), however smoothing is desirable for predictive purposes. When smoothing is present, the degree of bias depends critically on the type of spatial frequencies shared between the covariates and the spatial effect.

Spatial frequencies refer to the rate of variation of spatial patterns across the domain: higher spatial frequencies correspond to rapidly varying patterns, while lower spatial frequencies correspond to slowly varying, smooth patterns. Shared high frequencies between spatial effect and covariate are more problematic because spatial smoothing penalties disproportionately penalize high-frequency components in the spatial effect, leading to greater bias in the covariate’s estimated coefficient. In contrast, shared low frequencies are less influential as they experience weaker penalization (Dupont et al., 2023). These findings align with earlier insights by Paciorek (2010), who emphasized the risks of spatial effects operating at “smaller scales” than spatial covariates, and the role of smoothing as a bias inducer. Recently, in the spectral domain, Guan et al. (2022) developed a model that assumes that spatial confounding vanishes at high spatial frequencies. A variety of work has followed similar ideas (e.g. Mäkinen et al., 2022; Urdangarin et al., 2024). Note that broadly speaking, spatial scale and spatial frequency are inversely related: larger spatial scales correspond to lower spatial frequencies, and vice versa. In this paper, we use the term spatial frequency to align with recent work by Guan et al. (2022) and Dupont et al. (2023), and because it seems more precise.

In response to these challenges, numerous methods have been proposed to mitigate spatial confounding. Restricted spatial regression (RSR) (Reich et al., 2006; Hanks et al., 2015) was an early remedy, imposing orthogonality between the spatial effect and the covariates, thus leading to the same mean estimates for β as a non-spatial (NS) model. However, if the response is spatially varying, the NS model is misspecified and

the estimates of β might be biased. In addition, recent work (Khan and Calder, 2020; Zimmerman and Ver Hoef, 2021) shows that, contrary to expectations, the posterior variance of β can be smaller for RSR than for NS, ultimately also leading to worse coverage rates and higher Type-S errors (Gelman and Tuerlinckx, 2000).

Following these findings, alternative approaches have emerged, such as those by Dupont et al. (2022), Marques et al. (2022), or Guan et al. (2022). A particularly influential method is the spatial+ framework (Dupont et al., 2022), which has inspired numerous extensions (Marques and Kneib, 2022; Reich et al., 2022; Urdangarin et al., 2022, 2024; Schmidt, 2022). Spatial+ uses a two-stage frequentist approach: a spatial model is first fitted to the covariate, and the residuals from this model replace the covariate in a second-stage regression. Thus, ideally, the residuals that replace the covariate in the second stage equation should have sufficient *unconfounded* high spatial frequencies or non-spatial information such that β can still be identified.

While the spatial+ framework represents a significant advance in addressing spatial confounding, its frequentist implementation faces important limitations. This has led to subsequent modifications (Urdangarin et al., 2024; Dupont et al., 2023). For instance, spatial+ cannot guarantee there is no leakage of confounded spatial frequencies from the first stage to the second stage model. To improve this, Dupont et al. (2023) employ the same basis functions for spatial effects in both modeling stages but cap the number of high frequencies and set the first-stage smoothness parameter to zero – though the choice of this cap remains non-trivial. Moreover, inference procedures for spatial+ have not yet been formally developed. Schmidt (2022) propose a Bayesian variant using Gaussian processes instead of splines, which facilitates inference but does not resolve the issues related to frequency leakage. Finally, Marques and Kneib (2022) suggest a joint Bayesian formulation to propagate uncertainty from the first stage to the second.

This paper extends the spatial+ framework into a Bayesian setting through a joint model. By introducing a novel joint prior for smoothness-related components, we address key limitations of the frequentist approach. Our method offers several advantages: (i) enhanced uncertainty quantification (UQ) through joint estimation that properly propagates uncertainty across model stages; (ii) straightforward inference for all model parameters within the Bayesian paradigm; and (iii) prior restrictions that guarantee no frequency leakage – rather than restrictions on the posterior, like methods such as RSR. Specifically, our Bayesian framework employs a joint prior that controls the smoothness-related parameters of spatial effects for both the covariate and response. This eliminates the need for users to specify a frequency cap – a challenging task. Additionally, it mitigates issues associated with highly rank-deficient spatial effects, which can inflate uncertainty in β and diminish predictive performance. Importantly, we introduce a novel approach to Bayesian feedback that prevents oversmoothing of the second-stage spatial effect, thereby avoiding bias, leading to much improved results.

The paper is organized as follows. Section 2 reviews the spatial+ method of Dupont et al. (2022). Section 3 introduces the Bayesian spatial+ model, presenting our main contributions: novel joint priors for smoothness parameters that eliminate the need for user-specified frequency caps and prevent frequency leakage and a novel cutting feedback mechanism designed for this particular model. The extension to multiple covariates is

also discussed. Section 4 evaluates the model’s performance in two simulation studies, demonstrating substantial improvements in bias reduction and coverage over existing methods. Finally, Section 5 presents applications to meteorological and forestry data that validate our approach in real-world settings, before we conclude in Section 6.

2 Spatial+ in a nutshell

Consider a single observed covariate x and assume that both covariate and response are centered, so that we can omit intercepts. Our starting point is the spatial+ model of Dupont et al. (2022), which is formulated as a two-stage regression

$$\begin{aligned} x(\mathbf{s}_i) &= f^x(\mathbf{s}_i) + \varepsilon^x(\mathbf{s}_i), \\ y(\mathbf{s}_i) &= \beta(x(\mathbf{s}_i) - \hat{f}^x(\mathbf{s}_i)) + f(\mathbf{s}_i) + \varepsilon(\mathbf{s}_i) = \beta\hat{\varepsilon}^x(\mathbf{s}_i) + f(\mathbf{s}_i) + \varepsilon(\mathbf{s}_i), \end{aligned} \tag{1a}$$

where f and f^x are smooth functions on the spatial domain $\mathcal{S} \subseteq \mathbb{R}^2$ evaluated at locations $\mathbf{s}_i \in \mathcal{S}$, and $\varepsilon^x(\mathbf{s}_i) \stackrel{iid}{\sim} N(0, \sigma_x^2)$, $\varepsilon(\mathbf{s}_i) \stackrel{iid}{\sim} N(0, \sigma^2)$ are independent random errors. The term $\hat{f}^x(\mathbf{s})$ denotes the fitted values of $f^x(\mathbf{s})$ from (1a), and $\hat{\varepsilon}^x(\mathbf{s}_i) = x(\mathbf{s}_i) - \hat{f}^x(\mathbf{s}_i)$ are the corresponding residuals. In Dupont et al. (2022), and subsequent work, f and f^x are estimated using thin plate regression splines (TPRS, Wood, 2003).

The key idea is that the residuals $\hat{\varepsilon}^x$ are dominated by high-frequency spatial and non-spatial variation in x and therefore serve as a proxy for the unconfounded component of the covariate. Using these residuals in the second stage is reasonable as long as they retain enough information to identify β . Thus, the performance of spatial+ hinges on two conditions. Condition 1 (C1) $\hat{\varepsilon}^x$ must contain sufficient non-spatial or high-frequency information to identify β in the second stage, and Condition 2 (C2) the high-frequency components in $\hat{\varepsilon}^x$ must not be confounded with the spatial effect f .

C1 may fail for very smooth spatial covariates with little non-spatial variation, such as climate variables like air temperature, where $\hat{\varepsilon}^x$ may not be informative enough to identify β . More critically, C2 cannot be guaranteed without additional assumptions as the original spatial+ framework does not prevent leakage of shared high-frequency components between the covariate residuals and the spatial effect in the response (see Dupont et al., 2023; Urdangarin et al., 2024).

3 Bayesian Spatial+

In this section, we develop a Bayesian joint modeling version of spatial+, designed to

- (i) propagate uncertainty from the covariate model to the response model,
- (ii) enforce separation of high spatial frequencies between covariate residuals and the response level spatial effect through a joint smoothness prior, while controlling feedback in the joint model, and
- (iii) provide straightforward posterior inference for all model components.

We first introduce the joint model specification, then describe the basis representation and reparameterization we use. Building on this, we construct a joint smoothness prior that guarantees frequency separation between the residual and the response-level spatial effect. We then discuss feedback in the joint model and strategies to control it, before we turn to estimation and extensions.

3.1 A joint model specification

We consider a response $y(\cdot)$ defined on a spatial domain $\mathcal{S} \subseteq \mathbb{R}^2$ and, initially, a single spatial covariate $x(\cdot)$ (we lift this restriction in Section 3.6). As before, we assume that covariate and response are centered, so that intercepts can be omitted. Let

$$\mathbf{y} = (y(\mathbf{s}_1), \dots, y(\mathbf{s}_n))^\top \quad \text{and} \quad \mathbf{x} = (x(\mathbf{s}_1), \dots, x(\mathbf{s}_n))^\top.$$

The Bayesian spatial+ model replaces the plug-in residuals from the frequentist two stage approach by a joint model for both the covariate and response. We model

$$x(\mathbf{s}_i) = f^x(\mathbf{s}_i) + \varepsilon^x(\mathbf{s}_i), \quad \varepsilon^x(\mathbf{s}_i) \stackrel{iid}{\sim} N(0, \sigma_x^2), \quad (2a)$$

$$y(\mathbf{s}_i) = \beta \varepsilon^x(\mathbf{s}_i) + f(\mathbf{s}_i) + \varepsilon(\mathbf{s}_i), \quad \varepsilon(\mathbf{s}_i) \stackrel{iid}{\sim} N(0, \sigma^2), \quad (2b)$$

for $i = 1, \dots, n$, where f^x and f are smooth spatial effects and $\varepsilon(\mathbf{s}_i)$ and $\varepsilon^x(\mathbf{s}_i)$ are the latent residuals from the response model and covariate model, respectively. Importantly, $\varepsilon^x(\mathbf{s}_i)$ is not sampled; it is obtained as the difference $\varepsilon^x(\mathbf{s}_i) = x(\mathbf{s}_i) - f^x(\mathbf{s}_i)$, since treating noisy draws of $\varepsilon^x(\mathbf{s}_i)$ as covariates would inflate uncertainty and can bias regression coefficients (Carroll et al., 2006).

In vector form, with $\boldsymbol{\varepsilon}^x = (\varepsilon^x(\mathbf{s}_1), \dots, \varepsilon^x(\mathbf{s}_n))^\top$ and $\boldsymbol{\varepsilon} = (\varepsilon(\mathbf{s}_1), \dots, \varepsilon(\mathbf{s}_n))^\top$, this can be written as

$$\mathbf{x} = \mathbf{f}^x + \boldsymbol{\varepsilon}^x \quad \text{and} \quad \mathbf{y} = \beta \boldsymbol{\varepsilon}^x + \mathbf{f} + \boldsymbol{\varepsilon},$$

where $\mathbf{f}^x = (f^x(\mathbf{s}_1), \dots, f^x(\mathbf{s}_n))^\top$ and $\mathbf{f} = (f(\mathbf{s}_1), \dots, f(\mathbf{s}_n))^\top$.

This joint formulation makes explicit that the same latent residual process $\boldsymbol{\varepsilon}^x$ drives both the covariate model (2a) and the covariate contribution to the response model (2b). Compared to the frequentist spatial+ model, there is no plug-in estimate \hat{f}^x and no deterministic residual vector. Instead, uncertainty about f^x – and hence about the residual process $\boldsymbol{\varepsilon}^x$ – is fully propagated to inference on β .

We complete the model by assigning priors to the regression coefficient, variance parameters and spatial effects. Specifically, we let

$$\beta \sim N(0, \theta_\beta^2), \quad \sigma \sim \text{HN}(0, \theta_\sigma^2), \quad \sigma_x \sim \text{HN}(0, \theta_{\sigma_x}^2),$$

where $\text{HN}(0, \theta_*^2)$ denotes a half-normal distribution with scale $\theta_* > 0$. The spatial effects f and f^x are represented via a common spline basis, with corresponding coefficients and smoothness parameters. The basis representation and the associated reparameterization are described in the next subsection, while the joint smoothness prior is developed in Section 3.3.

3.2 Basis representation and reparameterization

3.2.1 Basis representation

A popular way of approximating spatially varying functions is via bivariate basis function approaches (Ramsay, 2002; Wood, 2003; Sangalli et al., 2013; Ugarte et al., 2017). We represent f and f^x in (2a) and (2b) using a common system of spatial basis functions. Let $\{B_j(\cdot)\}_{j=1}^d$ denote such a basis on \mathcal{S} and define

$$f(\mathbf{s}) = \sum_{j=1}^d \gamma_j B_j(\mathbf{s}), \quad f^x(\mathbf{s}) = \sum_{j=1}^d \gamma_j^x B_j(\mathbf{s}),$$

with coefficient vectors $\boldsymbol{\gamma} = (\gamma_1, \dots, \gamma_d)^\top$ and $\boldsymbol{\gamma}^x = (\gamma_1^x, \dots, \gamma_d^x)^\top$. Let \mathbf{Z} be the $n \times d$ design matrix with entries $Z_{ij} = B_j(\mathbf{s}_i)$, so that $\mathbf{f} = \mathbf{Z}\boldsymbol{\gamma}$ and $\mathbf{f}^x = \mathbf{Z}\boldsymbol{\gamma}^x$.

Following standard penalized spline practice, we associate a quadratic penalty matrix \mathbf{K} with the basis $\{B_j\}$ and use a smoothness parameter λ to control the overall roughness of f . In frequentist penalized regression, this yields a penalty term $\lambda \boldsymbol{\gamma}^\top \mathbf{K} \boldsymbol{\gamma}$. In the Bayesian setting, the corresponding (potentially improper) prior is

$$\boldsymbol{\gamma} \mid \tau^2 \propto (\tau^2)^{-r/2} \exp\left(-\frac{1}{2\tau^2} \boldsymbol{\gamma}^\top \mathbf{K} \boldsymbol{\gamma}\right),$$

with $r = \text{rank}(\mathbf{K}) \leq d$ and $\lambda = \sigma^2/\tau^2$ linking the frequentist smoothing parameter to the prior variance τ^2 (see Nychka, 2000). An analogous construction is used for $\boldsymbol{\gamma}^x$ with variance τ_x^2 and smoothing parameter $\lambda_x = \sigma_x^2/\tau_x^2$.

3.2.2 Reparameterization and spatial frequencies

For many spline bases such as TPRS, the penalty matrix \mathbf{K} measures the roughness of the function and can be viewed as a discrete approximation to a continuous roughness penalty. The matrix is typically rank deficient ($r < d$) as it is setup not to regulate specific low-frequency components such as the linear part.

Therefore, we can split the coefficient vector into penalized and unpenalized components by reparameterizing

$$\boldsymbol{\gamma} = \tilde{\mathbf{V}}\boldsymbol{\gamma}_{\text{pen}} + \tilde{\mathbf{U}}\boldsymbol{\gamma}_{\text{unpen}}, \quad (3)$$

where the $d \times r$ matrix $\tilde{\mathbf{V}}$ and the $d \times (d-r)$ matrix $\tilde{\mathbf{U}}$ can be obtained from the spectral decomposition of \mathbf{K} . $\tilde{\mathbf{U}}$ spans the null-space of \mathbf{K} and the matrices satisfy $\tilde{\mathbf{V}}^\top \mathbf{K} \tilde{\mathbf{V}} = \mathbf{I}_r$ and $\tilde{\mathbf{U}}^\top \mathbf{K} \tilde{\mathbf{U}} = \mathbf{0}$ (e.g. Wand, 2000; Fahrmeir et al., 2004). By construction, the vector $\boldsymbol{\gamma}_{\text{unpen}}$ operates on the unpenalized null space of \mathbf{K} and while $\boldsymbol{\gamma}_{\text{pen}}$ operates on the penalized complement. We obtain $\boldsymbol{\gamma}^\top \mathbf{K} \boldsymbol{\gamma} = \boldsymbol{\gamma}_{\text{pen}}^\top \boldsymbol{\gamma}_{\text{pen}}$ and assign priors

$$\boldsymbol{\gamma}_{\text{pen}} \mid \tau^2 \sim N(\mathbf{0}, \tau^2 \mathbf{I}_r), \quad p(\boldsymbol{\gamma}_{\text{unpen}}) \propto 1,$$

yielding a proper prior on the penalized component and a flat prior on the unpenalized part. The penalized component now has a well-behaved prior, while the flat prior on the

unpenalized component remains improper but is generally unproblematic. Under mild conditions on the rank of the design matrices and the priors on the variance components, the posterior remains proper even if \mathbf{K} is rank deficient (see Fahrmeir and Kneib, 2009; Klein et al., 2015).

The same construction is used for the covariate effect, with

$$\boldsymbol{\gamma}^x = \tilde{\mathbf{V}}\boldsymbol{\gamma}_{\text{pen}}^x + \tilde{\mathbf{U}}\boldsymbol{\gamma}_{\text{unpen}}^x,$$

and analogous priors for $\boldsymbol{\gamma}_{\text{pen}}^x$ and $\boldsymbol{\gamma}_{\text{unpen}}^x$ but conditional on τ_x^2 instead of τ^2 . In terms of the implied basis for the spatially varying functions, we obtain

$$\mathbf{f} = \mathbf{V}\boldsymbol{\gamma}_{\text{pen}} + \mathbf{U}\boldsymbol{\gamma}_{\text{unpen}} \quad \text{and} \quad \mathbf{f}^x = \mathbf{V}\boldsymbol{\gamma}_{\text{pen}}^x + \mathbf{U}\boldsymbol{\gamma}_{\text{unpen}}^x,$$

with $\mathbf{U} = \mathbf{Z}\tilde{\mathbf{U}}$ and $\mathbf{V} = \mathbf{Z}\tilde{\mathbf{V}}$. Although both \mathbf{f} and \mathbf{f}^x use the same basis functions, the associated coefficients are identified; see Proposition S.1 in Supplement ?? for a proof. Using the same basis functions guarantees that \mathbf{f} and \mathbf{f}^x are constructed from the same set of spatial frequencies, which is crucial for comparing and controlling their contributions.

3.3 A joint smoothness prior and frequency separation

3.3.1 Shrinkage of high frequencies

To gain insight into the shrinkage, consider the spectral decomposition $\mathbf{K} = \mathbf{\Gamma}\mathbf{\Omega}\mathbf{\Gamma}^\top$, where the diagonal matrix $\mathbf{\Omega} = \text{diag}(\omega_1, \dots, \omega_d)$ contains eigenvalues ordered by decreasing magnitude and $\mathbf{\Gamma}$ contains the corresponding eigenvectors. Let $\mathbf{\Omega}^+$ be the diagonal matrix constructed from the first r non-zero eigenvalues and let $\mathbf{\Gamma}^+$ be the corresponding submatrix of eigenvectors. Then $\tilde{\mathbf{V}} = \mathbf{\Gamma}^+(\mathbf{\Omega}^+)^{-1/2}$ while $\tilde{\mathbf{U}}$ is a basis of the null space of \mathbf{K} (see Fahrmeir et al., 2004; Klein et al., 2016, for details). Consider, an alternative but equivalent parameterization to (3). Writing $\tilde{\boldsymbol{\gamma}}_{\text{pen}} = (\mathbf{\Omega}^+)^{-1/2}\boldsymbol{\gamma}_{\text{pen}}$, the prior becomes $\tilde{\boldsymbol{\gamma}}_{\text{pen}} \mid \tau^2 \sim N(\mathbf{0}, \tau^2(\mathbf{\Omega}^+)^{-1})$, making explicit that components corresponding to larger eigenvalues ω_j receive smaller prior variance τ^2/ω_j .

Each eigenvector $\boldsymbol{\delta}_j$ of \mathbf{K} induces a spatial mode $\mathbf{m}_j = \mathbf{Z}\boldsymbol{\delta}_j$ and we can decompose the penalized part of \mathbf{f} as a sum of weighted modes $\mathbf{Z}\mathbf{\Gamma}^+\tilde{\boldsymbol{\gamma}}_{\text{pen}} = \sum_{j=1}^r \tilde{\gamma}_{\text{pen},j}\mathbf{m}_j$. For roughness-based penalties, modes associated with larger ω_j exhibit higher spatial frequency than those with smaller eigenvalues. Consequently, higher spatial frequency patterns receive strong shrinkage (Dupont et al., 2023).

3.3.2 A joint prior for frequency separation

The key idea of Bayesian spatial+ is to use a joint prior on the smoothness-related parameters to enforce that f^x to capture all lower spatial frequencies also present in f . Consequently, the residuals $\varepsilon^x = x - f^x$ contain high-frequency variation that f^x is too smooth to absorb and, thus, the even smoother f cannot absorb, and therefore, providing an unconfounded source of information for identifying β .

We parameterize smoothness in terms of the usual ratios

$$\lambda = \frac{\sigma^2}{\tau^2}, \quad \lambda_x = \frac{\sigma_x^2}{\tau_x^2}.$$

Our goal is to impose $\lambda_x < \lambda$, i.e., to ensure that the response effect is smoothed at least as strongly as the covariate effect. Rather than constraining λ and λ_x directly, we construct a prior on the variance parameters (τ^2, τ_x^2) that implies this ordering. Specifically, we set

$$\tau_x^2 = \tau^2 \frac{\sigma_x^2}{\sigma^2} (1 + \xi_x^2), \quad \xi_x \sim \text{HN}(0, \theta_x^2), \quad (4)$$

with fixed scale $\theta_x > 0$ in the half-normal prior, so $\lambda_x = \lambda/(1 + \xi_x^2) < \lambda$ almost surely. Under this prior, f is always at least as smooth as f^x , and typically more so. Consequently, the residuals ε^x preserve higher-frequency components that cannot be captured by f .

To understand the relevance of this ordering, consider three cases

1. If $\lambda < \lambda_x$, then f^x is smoother than f , and ε^x may retain spatial frequencies that remain confounded with f .
2. If $\lambda = \lambda_x$, the two spatial effects have identical smoothness. In principle this can avoid confounding, but joint estimation tends to be unstable when the data-generating smoothness of f and f^x differ.
3. If $\lambda > \lambda_x$, the residuals ε^x retain high-variation that f cannot absorb, reducing spatial confounding. Extreme choices such as $\lambda_x = 0$ (no smoothing for f^x) guarantee orthogonality at the cost of discarding potentially informative structure in x required for successful identification of β (see condition C1 in Section 2).

Our prior (4) implements the third case in a flexible way. Instead of capping the frequencies in the basis representation, it preserves the full basis for both effects while regulating their relative smoothness through the latent variable ξ_x . Section 3.5 discusses the weakly informative priors placed on (σ, σ_x, τ) . Under mild conditions, all hyperparameters are identified; see Proposition S.2 in the Supplement for details.

3.4 Feedback and how to control it

The joint smoothness prior introduces a deliberate dependence between the covariate and response models. This dependence is crucial for frequency separation, but it also creates a feedback mechanism in the joint posterior. Information from the covariate model can influence the effective amount of smoothing in the response model. In particular, if this mechanism makes the response model overly smooth then bias will be introduced (Paciorek, 2010; Dupont et al., 2022, 2023).

The joint prior enforces $\lambda_x = \lambda/(1 + \xi_x^2) < \lambda$ and thus links the covariate-side smoothing to the response-side smoothing via the relationship among σ , τ and τ_x . When the data for x favor very smooth effects (e.g., large λ_x ; see Scenario 2 in Section 4.1), the

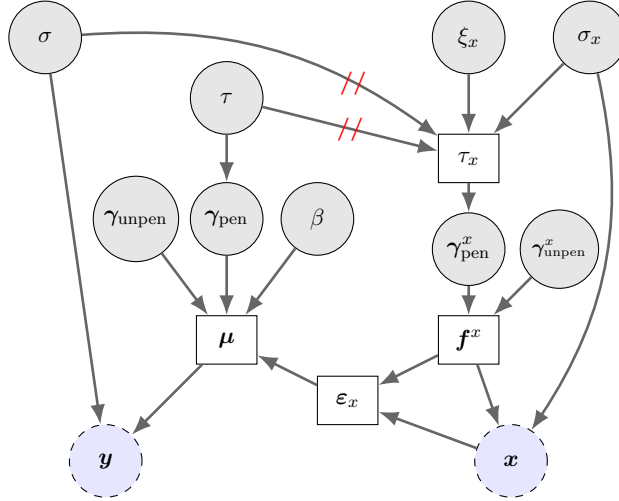


Figure 1: Graphical model representation of the Bayesian spatial+ model. Random variables appear as gray circles with incoming arrows indicating conditional dependencies. The two pale blue dashed circles at the bottom represent the observed data y and x . Boxes denote deterministic transformations, with incoming arrows indicating the variables they depend on. For example, $\boldsymbol{\mu} = \mathbf{x}\boldsymbol{\beta} + \mathbf{V}\boldsymbol{\gamma}_{\text{pen}} + \mathbf{U}\boldsymbol{\gamma}_{\text{unpen}}$. The graphical structure reveals a problematic feedback channel from the covariate model to the response model as the prior for $\boldsymbol{\gamma}_{\text{pen}}^x$ depends on τ and σ through τ_x . We eliminate this feedback (red bars indicate cut connections) by treating τ_x as fixed when updating (σ, τ) , effectively removing the influence of $p(\boldsymbol{\gamma}_{\text{pen}}^x | \tau_x)$ on these parameters.

posterior for (σ, τ) may move towards configurations that increase λ . In other words, this creates a feedback channel through which the covariate model can push the response model towards stronger smoothing than would be justified by y alone. If f becomes too smooth, it can push spatial signal into β and re-introduce bias. This is an instance of Bayesian feedback (e.g., McCandless et al., 2009; Stephens et al., 2023), where information flows between submodels through shared parameters. Figure 1 visualizes these relationships in a graphical model.

Our approach is to cut feedback (McCandless et al., 2009) by preventing the covariate model from updating the response-side smoothness-related parameters (σ, τ) . Conceptually, we retain the joint prior structure that ensures $\lambda_x < \lambda$, but we block the contribution of the covariate model to inference on (σ, τ) . Figure 1 makes this dependency entanglement explicit in terms of a graphical model representation. Arrows indicate the dependence of $\boldsymbol{\gamma}_{\text{pen}}^x$ on (σ, τ) via the deterministic transformation τ_x . For inference on (σ, τ) , we treat τ_x as fixed, which corresponds to removing the arrows from σ and τ to τ_x and thus removing the feedback from $\boldsymbol{\gamma}_{\text{pen}}^x$ to those parameters, so that the posterior for (σ, τ) is driven by the response model alone. This preserves Bayesian coherence for all parameters except (σ, τ) , but removes the problematic feedback channel and avoids

oversmoothing driven by x . We argue that this sacrifice of coherence is justified since our goal is not to find the optimal model for x but rather ensure that the problematic, i.e. shared, frequencies are removed from it.

Our technique diverges from a traditional cut-feedback model – typically motivated by causal inference. In our model, (τ, σ) are the only parameters in the prior hierarchy of y that also appear in the hierarchy of x . A traditional cut-feedback approach would discard all information from the response model when estimating (σ, τ) , whereas we do the reverse by blocking information from the covariate model. Since (τ, σ) appear in the model for x only through the derived parameter $\tau_x^2 = \tau^2 \frac{\sigma_x^2}{\sigma^2} (1 + \xi_x^2)$, these hyperparameters become unidentifiable under the traditional approach. In Supplement ??, we confirm that the traditional cut-feedback approach does not work in our model: it produces extremely large standard errors (even on the log-scale) and systematically achieves coverage rates of 1, confirming the severe identifiability issues inherent in this approach.

3.5 Estimation and Computational Details

We perform Bayesian inference using Markov chain Monte Carlo (MCMC). The unobserved model parameters comprise

$$\beta, \gamma_{\text{pen}}, \gamma_{\text{unpen}}, \gamma_{\text{pen}}^x, \gamma_{\text{unpen}}^x, \sigma, \sigma_x, \tau, \xi_x$$

and, in the prior-bounded model, we have λ_{sp} and ξ_λ instead of τ . We employ a Metropolis-Hastings within Gibbs scheme. The parameters blocks comprise of a block of spline and regression coefficients of the response model $(\beta, \gamma_{\text{pen}}, \gamma_{\text{unpen}})$, a block spline coefficients of the covariance model $(\gamma_{\text{pen}}^x, \gamma_{\text{unpen}}^x)$ and a block of hyperparameters $(\sigma, \sigma_x, \tau, \xi_x, \lambda_{\text{sp}})$. For the coefficient blocks, we use iteratively weighted least squares (IWLS) proposals (Gamerman, 1997). Hyperparameters are updated on unrestricted domains (logarithmic transformation for positive parameters) using Hamiltonian Monte Carlo (HMC, Neal, 2011). This blocking strategy and use of IWLS proposals is following practices established in software for Bayesian regression such as BayesX (Brezger et al., 2005).

All models are implemented in Python using `liesel` (Riebl et al., 2022), a probabilistic programming framework based on JAX and BlackJAX (Bradbury et al., 2024; Cabezas et al., 2024). Besides full control over the model specification, the framework provides the flexibility needed for model specific MCMC algorithms such as the cut-feedback mechanism. Such customization would be challenging or impossible to implement in many standard frameworks such as STAN (Stan Development Team, 2023). We assess convergence using standard diagnostics such as the \hat{R} statistic and effective sample sizes (Gelman and Hill, 2006; Vehtari et al., 2021).

We place half-normal priors on the hyperparameters. These are weakly informative shrinkage priors that keep hyperparameters close to zero when the data are weak, while avoiding the pathological posterior curvature that can arise from overly diffuse or heavy-tailed priors. This regularizes the posterior and leads to more stable Hamiltonian Monte Carlo geometry. In addition, the half-normal distribution has support on the

positive reals, which is appropriate for these scale parameters. Throughout the numerical experiments, we set all scale parameters in the priors on the hyperparameters to 10, except $\theta_{\xi_x} = 1$ yielding stronger regularization toward zero for ξ_x . This tighter prior on ξ_x ensures that f^x does not become overly flexible and ε^x retains essential high-frequency information, while the model setup always maintains the ordering constraint $\lambda_x < \lambda$. These hyperparameter values assume that parameters are approximately on unit scale after centering (see Gelman, 2006; Gelman et al., 2013, for a more detailed discussion of priors for variance parameters).

To model the spatial effects f and f_x , we use thin plate regression splines, a low-rank approximation of thin plate splines (Wood, 2003, see Section 3.6.1). Additional details on MCMC diagnostics are provided alongside the simulations and applications. The complete model hierarchy is shown in Supplement ??.

3.6 Variants and Extensions

This section presents extensions and variants of our methodology. Initially, we discuss thin plate regression splines, which we use for computational efficiency in the simulations and applications. Then, we introduce an alternative to cutting feedback when coherence is a primary concern and extend the model to multiple covariates.

3.6.1 Thin plate regression splines

For computational efficiency, we use thin plate regression splines (TPRS, Wood, 2003), which approximate the corresponding thin plate splines (Engle et al., 1986; Wahba, 1984) by the best rank- k approximation in the spectral sense. In a nutshell, this means that the regression spline basis is obtained from a spectral decomposition of the thin plate spline kernel at the data locations, retaining only k eigencomponents corresponding to the smoothest (low-frequency) directions, together with low-order polynomial functions (e.g. linear functions of the input coordinates). Additionally, the penalty is constructed from a roughness based penalty and includes in its null space the low-order polynomial component, which induces rank deficiency in the penalty matrix.

3.6.2 Prior-bounded λ

If coherence is of higher concern, we introduce an alternative to cutting feedback using Empirical Bayes. We consider bounding the response-side smoothing from above by using an informative prior effectively limiting λ . We introduce an upper bound $\lambda_{\text{sp}} > 0$ and parameterize

$$\tau^2 = \sigma^2 \left(\frac{1}{\lambda_{\text{sp}}} + \xi_\lambda^2 \right), \quad \xi_\lambda \sim \text{HN}(0, \theta_\tau^2),$$

which enforces $\lambda = \sigma^2/\tau^2 < \lambda_{\text{sp}}$ while allowing less shrinkage through ξ_λ^2 . When sufficient prior knowledge is present, fixing the bound λ_{sp} is an option, otherwise λ_{sp} is itself treated as a random quantity with an (weakly) informative prior. The bound λ_{sp} is calibrated using posterior inference from a standard spatial model (see Supplement ?? for concrete

details). This prior-bounded version maintains a coherent joint posterior and limits oversmoothing by restricting how large λ may become. The complete model hierarchy is shown in Supplement ???. In our empirical studies, both strategies reduce oversmoothing and bias, with the cut-feedback model typically providing the most robust performance.

3.6.3 Multiple covariates

The methodology developed above naturally extends to multiple spatially-varying covariates. Consider p covariates $x_q(\mathbf{s})$, $q = 1, \dots, p$. We naturally extend (2b) to

$$y(\mathbf{s}_i) = \sum_{q=1}^p \beta_q \varepsilon_q^x(\mathbf{s}_i) + f(\mathbf{s}_i) + \varepsilon(\mathbf{s}_i)$$

where the residual of each covariate model is created as in (2a), i.e., $x_q(\mathbf{s}_i) = f_q^x(\mathbf{s}_i) + \varepsilon_q^x(\mathbf{s}_i)$ with independent priors on the residual variance.

Following the preceding sections, we use common basis functions for all spatial effects and perform the reparameterization on each and place the priors as described on the penalized coefficient with variance parameters $\tau_{x,q}^2$. Now, similarly to Equation (4) for each q we impose

$$\tau_{x,q}^2 = \tau^2 \frac{\sigma_{x,q}^2}{\sigma^2} (1 + \xi_{x,q}^2), \text{ with } \xi_{x,q} \sim \text{HN}(0, \theta_x^{q^2}), q = 1, \dots, p.$$

The prior specification ensures that each covariate's spatial effect smoothness $\lambda_{x,q} = \sigma_{x,q}^2 / \tau_{x,q}^2$ satisfies the smoothness restriction $\lambda_{x,q} < \lambda$, preventing that any covariate residual ε_q^x contains frequency patterns shared with f . The covariate-specific parameters driving $\tau_{x,q}^2$ are independent a-priori, allowing flexible smoothness control across covariates. Control over Bayesian feedback is achieved by the natural extension of Section 3.4 to the new setting. Similarly, for the prior-bound variant.

When dealing with p spatially aligned covariates, collinearity among covariates becomes a natural concern. While not the primary focus of our here, we recommend preprocessing with standard techniques such as principal component analysis or combining highly collinear covariates to reduce collinearity before model fitting (see Chapter 3 of Fahrmeir and Lang, 2001, for details). Once these preprocessing steps are completed, the methods proposed in this section can be applied more effectively. By reducing collinearity, the remaining covariates are expected to retain sufficient unique non-spatial or high-frequency spatial information, ensuring that each ε_q^x , $q = 1, \dots, p$, retain enough information to accurately recover the associated coefficient estimate β_q . An assessment of the effect of collinearity is provided in the simulation study in Section 4.2, with successful results for our proposed model.

4 Simulation studies

In this section, we demonstrate the performance of Bayesian spatial+ over the frequentist counterpart using synthetic data, by evaluating performance in terms of bias reduction,

coverage rates, and large-sample behavior. Section 4.1 considers the case of one covariate and Section 4.2 extends to two covariates. Initially, we consider one covariate and then extend to two covariates. The data setups are inspired by Dupont et al. (2022), Dupont et al. (2023) and Dupont and Augustin (2023).

We compare five models: a standard Bayesian spatial model (`spatial`), the frequentist spatial+ (`spatial+freq`), the Bayesian spatial+ without feedback control (`spatial+simple`), the prior-bounded Bayesian spatial+ variant (`spatial+hn`) from Section 3.6.2, and the Bayesian spatial+ with cut feedback (`spatial+cut`). We do not fit any non-spatial models, as these are misspecified when there is unobserved spatial variability in the data, which is the case for both scenarios (Gilbert et al., 2025).

All models use TPRS with 500 basis functions. A pragmatic approach to choose k is to increase k if the estimated degrees of freedom for a TPRS exceeds some specified proportion of the basis dimension, commonly 80% (see Wood, 2003). Frequentist models are fitted using `R-mgcv` (Wood, 2016) and Bayesian models using `Liesel` (Riebl et al., 2022). We use four MCMC chains, each with 2000 posterior samples and 3000 warm-up samples, and check the R-hat values based on MCMC chains for convergence (Gelman et al., 1992; Vehtari et al., 2021).

4.1 One covariate

We analyze spatial model performance across three scenarios using data at $n \in \{500, 1000\}$ locations sampled via Latin hypercube in $\mathcal{S} = [0, 1]^2$. For 100 replicates, we generate

$$\begin{aligned} y(\mathbf{s}_i) &= x(\mathbf{s}_i) + z_{high}(\mathbf{s}_i) + z_{low}(\mathbf{s}_i) + \varepsilon(\mathbf{s}_i), \\ x(\mathbf{s}_i) &= z(\mathbf{s}_i) + \varepsilon^x(\mathbf{s}_i) \end{aligned}$$

where $\varepsilon(\mathbf{s}_i) \sim N(0, 0.1^2)$ and $\varepsilon^x(\mathbf{s}_i) \sim N(0, \sigma_x^2)$. Moreover, z_{high} and z_{low} are high and low frequency fields corresponding to the fitted values of a TPRS model with 500 and 20 basis functions, respectively, to a realization of a Gaussian process with exponential covariance function $C_{exp}(h) = \exp(-(h/R^{exp}))$ with unit variance, where h is the Euclidean distance between two observation locations, R^{exp} (related to spatial range) is set to 0.3. Consider also the high frequency field z_{high2} generated similar to z_{high} but based on an independent realization of the underlying process. The scenarios differ in terms of $z(\mathbf{s}_i)$ and σ_x as specified in Table 1.

We expect Scenario 1 to lead to biased estimates of β (true value = 1) due to shared high frequencies between x and the response’s spatial effects (z_{high}). In Scenario 2, we

	$z(\mathbf{s}_i)$	σ_x
Scenario 1	$z_{high}(\mathbf{s}_i)$	0.1
Scenario 2	$z_{high}(\mathbf{s}_i)$	0.2
Scenario 3	$0.8z_{low}(\mathbf{s}_i) + 0.2z_{high2}(\mathbf{s}_i)$	0.1

Table 1: Specifications of the three simulation scenarios.

	spatial	spatial+freq	spatial+simple	spatial+hn	spatial+cut
Scenario 1	0.01	0.30	0.73	0.75	0.95
Scenario 2	0.08	0.17	0.48	0.58	0.90
Scenario 3	0.89	0.85	0.90	0.89	0.89

Table 2: Coverage rates for β based on 95% intervals ($n = 1000$).

increase the amount of non-spatial information through larger σ_x , which helps identify the effects and should reduce bias compared to Scenario 1. In Scenario 3, we expect minimal bias since confounding occurs only at low frequencies, which experience less penalization and thus cause less distortion in coefficient estimation.

Results For $n = 1000$, Figure 2 shows the bias and standard deviation of the estimate of β for the three scenarios. Table 2 shows the coverage rates for β based on 95% confidence/credible intervals. In Scenario 1, **spatial+cut** leads to the lowest bias and reaches the nominal coverage rate. The next closest models are **spatial+simple** and **spatial+hn** with 75% coverage, both outperforming the frequentist counterpart in terms of bias and coverage. The **spatial** model performs very poorly in both dimensions. Regarding convergence diagnostics, **spatial+simple** struggles with reaching the threshold R-hat values compared to **spatial+hn** and **spatial+cut**. As expected, increasing σ_x (Scenario 2) reduces bias in general. This scenario also clarifies the need to cut feedback since λ_x is pushed toward higher values as σ_x increases, potentially affecting λ via the constraint $\lambda_x < \lambda$. Both **spatial+hn** and **spatial+cut** achieve better coverage rates than **spatial+simple**, with **spatial+cut** proving more effective than **spatial+hn** in handling feedback. In Scenario 3, all models reach bias close to zero and have high coverage rates. The frequentist **spatial+** has a more noticeable positive bias, which could be explained by undersmoothing in the first stage that leads to residuals that are not very informative.

Results for $n = 500$ show similar bias patterns (see Supplement ??), though coverage rates are generally closer to the nominal level in the confounded scenarios. Figure 3 shows coverage rates as sample size increases. Notably, **spatial+cut** is the only method whose coverage is maintained with increasing n when confounding is present and is overall close to the nominal level. In contrast, other methods (except in the unconfounded scenario) exhibit deteriorating coverage as sample size grows. A typical pattern of biased estimators, where larger samples yield tighter intervals centered on biased estimates (see Supplement ??). This finding further supports the advantage of **spatial+cut**.

4.2 Two covariates

We assess model performance with two spatially aligned covariates using 100 replicates at $n = 1000$ locations (Latin hypercube sampling as above). Inspired by Dupont and

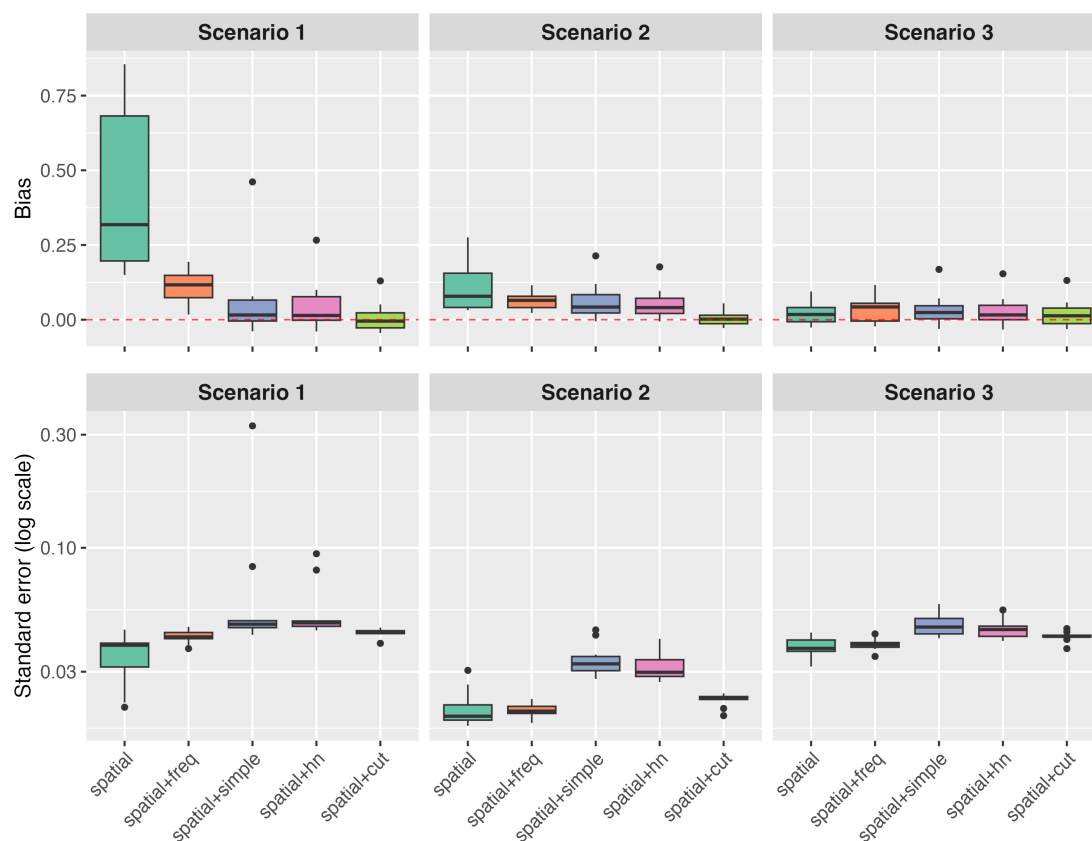


Figure 2: Bias estimate of β (top) and standard error in log-scale (bottom) for Scenarios 1, 2 and 3 for $n = 1000$.

Augustin (2023), data is generated according to

$$\begin{aligned}
 y(\mathbf{s}_i) &= 0.5x_1(\mathbf{s}_i) + 0.5x_2(\mathbf{s}_i) + z_{high}(\mathbf{s}_i) + z_{low}(\mathbf{s}_i) + \varepsilon(\mathbf{s}_i), \\
 x_1(\mathbf{s}_i) &= 0.5z_{high}(\mathbf{s}_i) + 0.5z_{high2}(\mathbf{s}_i) + \varepsilon_1^x(\mathbf{s}_i), \\
 x_2(\mathbf{s}_i) &= z(\mathbf{s}_i) + \varepsilon_2^x(\mathbf{s}_i)
 \end{aligned}$$

with $\varepsilon(\mathbf{s}_i) \sim N(0, 0.1^2)$ and $\varepsilon_1^x(\mathbf{s}_i), \varepsilon_2^x(\mathbf{s}_i) \sim N(0, 0.1^2)$. The values of z_{high} , z_{high2} , and z_{low} are generated analogously to the one covariate case. The scenarios differ in terms how $z(\mathbf{s}_i)$ is defined. In Scenario 1, define $z(\mathbf{s}_i) = 0.8z_{high}(\mathbf{s}_i) + 0.2z_{high2}(\mathbf{s}_i)$; in Scenario 2, define $z(\mathbf{s}_i) = 0.2z_{high}(\mathbf{s}_i) + 0.8z_{high2}(\mathbf{s}_i)$; in Scenario 3, define $z(\mathbf{s}_i) = 0.7z_{low}(\mathbf{s}_i) + 0.1z_{high}(\mathbf{s}_i) + 0.2z_{high2}(\mathbf{s}_i)$. The first scenario represents a setting where x_2 shares high frequencies with f and x_1 with a relatively large weight. In the second scenario, this weight drops to 0.2 for x_2 , such that we would expect generally smaller bias in β_2 . In Scenario 3, x_1 and x_2 are again not strongly correlated; f and x_2 share low frequencies through z_{low} with a weight of 0.7, but shared low frequencies lead to

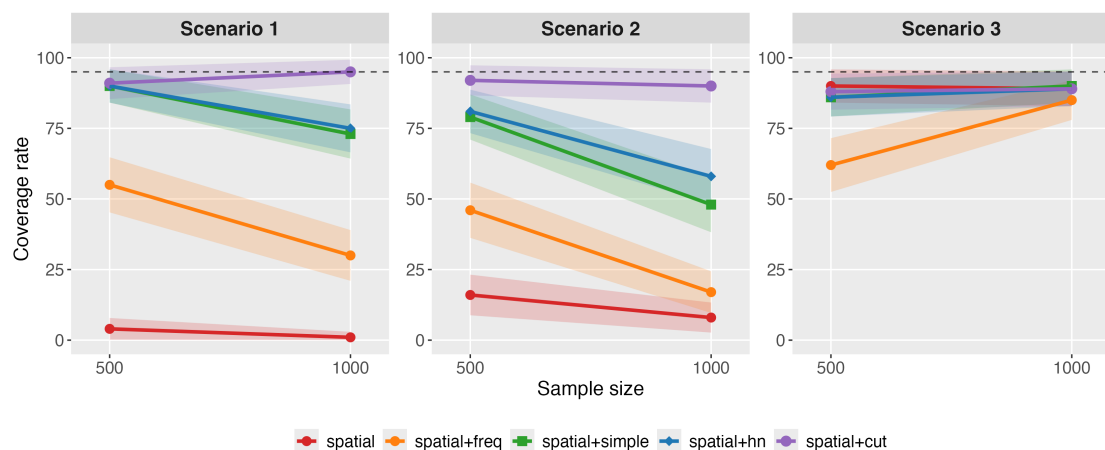


Figure 3: Coverage rates of intervals for one covariate as sample size increases from $n = 500$ to $n = 1000$. The shaded band represents the 95% confidence interval for the empirical coverage estimate, computed using a normal approximation with variance derived from the binomial distribution.

little to no spatial confounding.

Results Figure 4 and Table 3 present the bias and coverage results for both coefficients β_1 and β_2 (associated with x_1 and x_2 , respectively) across all three scenarios. **spatial+cut** consistently achieves the lowest median bias and highest coverage rates across all scenarios and coefficients, substantially outperforming the frequentist approach and standard spatial model. The estimates for β_1 remain stable across scenarios since x_1 maintains the same structure throughout, with optimal performance in Scenario 1 where both covariates are more noticeably confounded amongst themselves. In Scenario 2, x_2 suffers less from spatial confounding and most models improve, with the notable exception of **spatial+freq**, which exhibits similar bias to Scenario 1. This may be because the frequentist approach removes too much information from ε^x , making it difficult to accurately identify β_2 , or is not able to avoid frequency leakage from the first-stage. In Scenario 3, β_2 exhibits low bias across all models, as expected given the minimal spatial confounding in this setting. Still, the Bayesian spatial+ models do significantly better in terms of coverage of β_2 than the remaining models. Supplement ?? presents the standard errors associated with the estimates, showing that **spatial+freq** and **spatial+cut** achieve similar precision for the coefficient estimates, while **spatial+simple** and **spatial+hn** exhibit the largest standard errors.

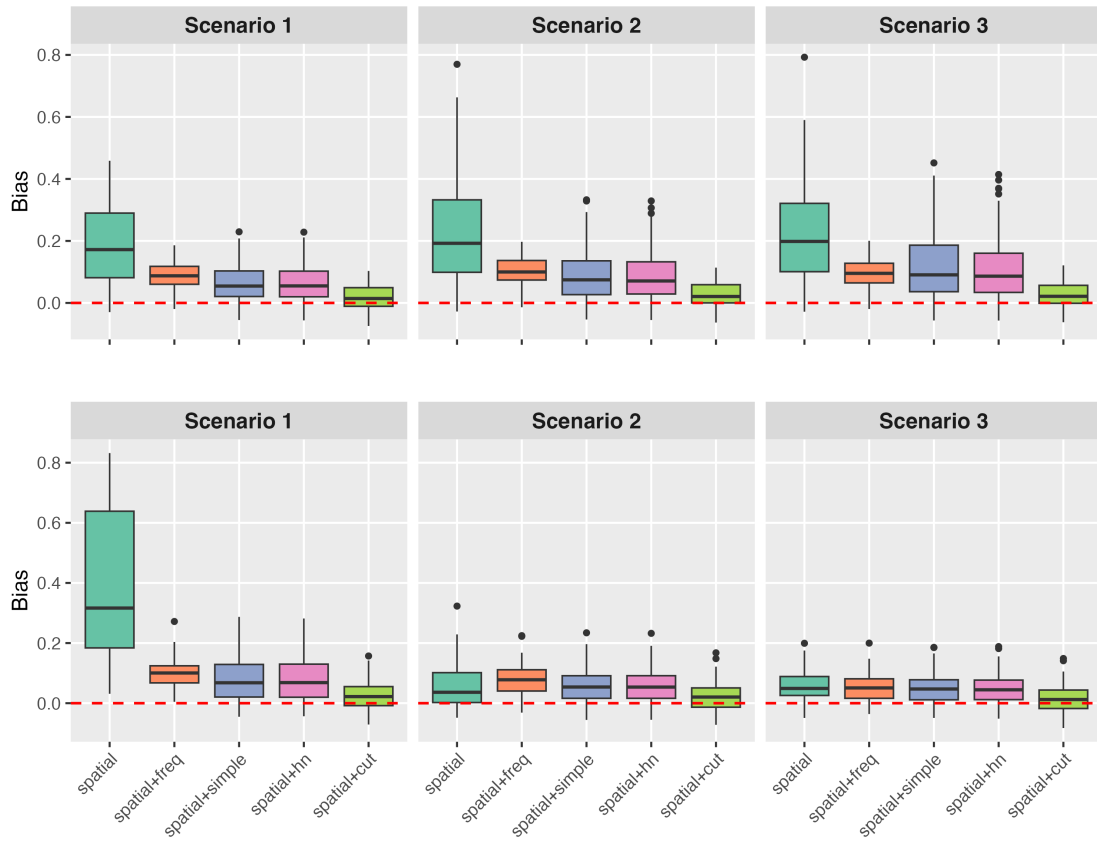


Figure 4: Bias estimate of β_1 (top) and β_2 (bottom) for Scenarios 1, 2 and 3.

5 Applications to real data

5.1 Average daily precipitation in Germany

We analyze the average amount of daily precipitation in February 2016 across Germany, using air temperature as a covariate. The dataset includes observations from 279 weather stations. We apply a square-root transformation to the rainfall variable to stabilize variance and then standardize all variables. Figure 5 illustrates the transformed and standardized variables. The scatterplots reveal a common smaller-scale spatial pattern between rainfall and air temperature. Specifically, lower temperatures are observed from the east to the central and southern regions of the country, coinciding with locations with larger amounts of precipitation. This pattern aligns with areas of higher altitude. Given the strong correlation between temperature and altitude, we chose not to include both variables simultaneously in the model.

	β_1			β_2		
	S1	S2	S3	S1	S2	S3
spatial	0.15	0.12	0.10	0.03	0.64	0.68
spatial+freq	0.44	0.32	0.38	0.42	0.55	0.73
spatial+simple	0.79	0.61	0.60	0.65	0.80	0.91
spatial+hn	0.78	0.62	0.61	0.66	0.80	0.91
spatial+cut	0.94	0.90	0.90	0.93	0.90	0.95

Table 3: Coverage rates for β_1 (left table) and β_2 (right table) based on 95% confidence/credible intervals ($n = 1000$). S1, S2 and S3 refer to Scenarios 1, 2 and 3.

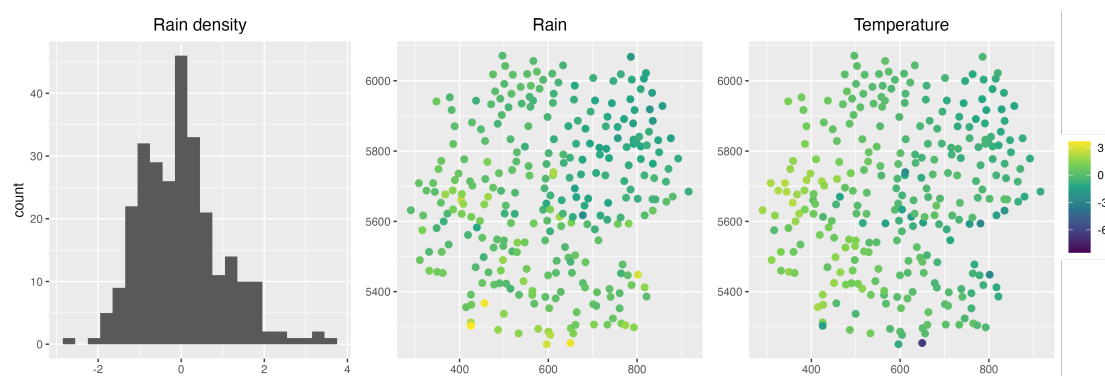


Figure 5: Histogram for the response rain (left); scatterplots for the transformed response, rainfall (center), and the covariate, air temperature (right).

Results We fit all models to the data using TPRS with 150 basis functions and use four MCMC chains, each with 2000 posterior samples and a warm-up comprised of 3000 iterations. Table 4 presents the confidence and credible intervals for the estimate of β_{temp} . The results indicate evidence of spatial confounding since the estimates of the models corrected for spatial confounding change compared to the spatial model. Relative to the standard spatial model ($\hat{\beta}_{temp} = -0.82$), `spatial+freq` shows increased magnitude ($\hat{\beta}_{temp} = -0.89$), while the Bayesian spatial+ methods achieve larger corrections ($\hat{\beta}_{temp} = -0.97$). The consistency across Bayesian spatial+ methods suggests robust bias correction, with `spatial+cut` performing similarly to `spatial+hn` and `spatial+simple`. These findings align with our simulation results, confirming that Bayesian spatial+ methods provide more effective spatial confounding correction than the frequentist approach. An $\hat{R} < 1.1$ indicates convergence.

5.2 Tree coverage in Germany

We revisit an application in Dupont et al. (2022, data provided in the supplementary material) and details on the original data are available at Augustin et al. (2009). The

dataset considers data on spruce trees collected in 2013, corresponding to $n = 186$ observation locations in Germany. We study the effect of minimum temperature in May (`temp`) and tree age (`age`) on crown defoliation (`defol`) expressed as a ratio. High minimum temperature in May is indicative of a warmer year which, in turn, is likely to lead to higher levels of tree defoliation (measured later in the summer). Moreover, it is expected that older trees have more defoliation. All variables are standardized. Figure 6 displays the fitted values of fitting a smooth TPRS to defoliation (left), age (center), and temperature (right), independently. The spatial components of defoliation and age are quite smooth and spatial TPRSs can only explain a small percentage of the deviances in the data (less than 13%). In contrast, the spatial structure of temperature appears considerably more complex and the TPRS explains about 76% of the deviance in the data.

Results We fit the models using 100 basis functions and for the Bayesian models run four MCMC chains with 2000 posterior samples and a warm-up of 3000 iterations. Convergence is verified using \hat{R} . Table 5 presents the estimated coefficient for the different models. The coefficients for temperature approximately double in magnitude for the `spatial+` models compared to the standard spatial model, while the coefficients for age are estimated consistently across all models. The results, consistent with Dupont et al. (2022), indicate that age is not affected by spatial confounding, but temperature is. The Bayesian and frequentist versions of the `spatial+` models give similar results, with `spatial+cut` having the smallest coefficient estimate and `spatial+freq` having the largest. The cut feedback method has a 8% smaller standard error compared with the frequentist counter part.

6 Discussion

This work brings the `spatial+` methodology to a Bayesian framework, offering three key advantages. First, we provide enhanced uncertainty quantification with seamless uncertainty propagation in the joint model. Second, this enables robust posterior inference beyond point estimates, addressing a gap in the original `spatial+` framework where inference beyond the mean was not explicitly detailed. Third, the Bayesian approach

	$\hat{\beta}_{temp}$	$se(\hat{\beta}_{temp})$	$CI(\beta_{temp})$
<code>spatial</code>	-0.82	0.0526	[-0.93, -0.71]
<code>spatial+freq</code>	-0.89	0.0663	[-1.02, -0.76]
<code>spatial+simple</code>	-0.97	0.0625	[-1.09, -0.85]
<code>spatial+hn</code>	-0.97	0.0611	[-1.09, -0.86]
<code>spatial+cut</code>	-0.97	0.0613	[-1.08, -0.85]

Table 4: Point estimate $\hat{\beta}_{temp}$ and corresponding standard error (se) and confidence/credibility intervals (CI) for all models.

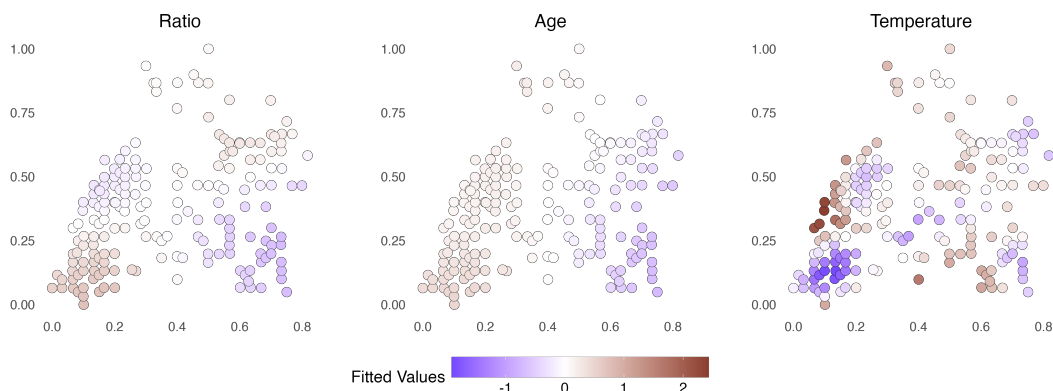


Figure 6: We fit thin plate regression splines applied to defoliation (left), age (center), temperature (right) using `mgcv` and show the fitted values of the spatial smooth; x and y the spatial coordinates.

	$\hat{\beta}_{age}$	se_{age}	$CI(\hat{\beta}_{age})$	$\hat{\beta}_{temp}$	$se(\hat{\beta}_{temp})$	$CI(\hat{\beta}_{temp})$
<code>spatial</code>	0.6787	0.0537	[0.5741, 0.7836]	0.1199	0.0602	[0.0022, 0.2381]
<code>spatial+freq</code>	0.6749	0.0529	[0.5704, 0.7793]	0.2694	0.0990	[0.0740, 0.4648]
<code>spatial+simple</code>	0.6854	0.0537	[0.5810, 0.7915]	0.2565	0.0981	[0.0636, 0.4519]
<code>spatial+hn</code>	0.6855	0.0535	[0.5801, 0.7909]	0.2560	0.0957	[0.0719, 0.4447]
<code>spatial+cut</code>	0.6848	0.0563	[0.5725, 0.7948]	0.2487	0.0929	[0.0655, 0.4301]

Table 5: Point estimates $\hat{\beta}_{temp}$ and $\hat{\beta}_{age}$ and the corresponding standard errors (se) and confidence/credibility intervals (CI) for all estimated models.

allows incorporating prior knowledge about spatial confounding, enabling restrictions that explicitly avoid confounded high frequencies. Additionally, we identify a feedback problem that emerges specifically in the joint Bayesian formulation and propose a cutting feedback approach that differs from traditional methods by selectively removing problematic dependencies from parameters in the response side. We extended the presented methodology to multiple covariates.

We evaluated our approach through simulation studies and applications to two real-world datasets with both single and multiple covariates. Results demonstrate that the Bayesian `spatial+` models, particularly the cutting feedback model, represent a substantial improvement over the frequentist counterpart in both bias and coverage, and the `spatial` model performed consistently worse than all `spatial+` models, except when there was no relevant confounding. Importantly, our approach achieves these improvements without requiring user-specified tuning parameters such as frequency caps, making it both more effective and more practical than existing alternatives. Nevertheless, the current requirement of separability between residuals and spatial effects presents challenges when extending `spatial+` to non-Gaussian covariates. Future research could focus on developing more flexible methodologies to address these limitations and further expand

the applicability of Bayesian spatial+.

Acknowledgements

We extend our gratitude to Thomas Kneib for helpful comments and discussions. We also acknowledge the valuable feedback received from editors and anonymous reviewers. IM acknowledges support by the Deutsche Forschungsgemeinschaft (DFG, German Research Foundation) through CRC 990 “Ecological and Socioeconomic Functions of Tropical Lowland Rainforest Transformation Systems”.

References

- Augustin, N. H., Musio, M., von Wilpert, K., Kublin, E., Wood, S. N., and Schumacher, M. (2009). Modeling spatiotemporal forest health monitoring data. *Journal of the American Statistical Association*, 104(487):899–911.
- Bradbury, J., Frostig, R., Hawkins, P., Johnson, M. J., and Leary, C. (2024). JAX: Autograd and XLA.
- Brezger, A., Kneib, T., and Lang, S. (2005). Bayesx: analyzing bayesian structural additive regression models. *Journal of Statistical Software*, 14:1–22.
- Cabezas, A., Corenflos, A., Lao, J., Louf, R., Carnec, A., Chaudhari, K., Cohn-Gordon, R., Coullon, J., Deng, W., Duffield, S., Durán-Martín, G., Elantkowski, M., Foreman-Mackey, D., Gregori, M., Iguaran, C., Kumar, R., Lysy, M., Murphy, K., Orduz, J. C., Patel, K., Wang, X., and Zinkov, R. (2024). BlackJAX: Composable Bayesian inference in JAX.
- Carroll, R. J., Ruppert, D., Stefanski, L. A., and Crainiceanu, C. M. (2006). *Measurement error in nonlinear models: a modern perspective*. Chapman and Hall/CRC.
- Clayton, D. G., Bernardinelli, L., and Montomoli, C. (1993). Spatial correlation in ecological analysis. *International Journal of Epidemiology*, 22(6):1193–1202.
- Dupont, E. and Augustin, N. H. (2023). Spatial confounding and spatial+ for nonlinear covariate effects. *Journal of Agricultural, Biological and Environmental Statistics*, pages 1–16.
- Dupont, E., Marques, I., and Kneib, T. (2023). Demystifying spatial confounding. *arXiv preprint arXiv:2309.16861*.
- Dupont, E., Wood, S. N., and Augustin, N. H. (2022). Spatial+: a novel approach to spatial confounding. *Biometrics*, 78(4):1279–1290.
- Engle, R. F., Granger, C. W., Rice, J., and Weiss, A. (1986). Semiparametric estimates of the relation between weather and electricity sales. *Journal of the American Statistical Association*, 81(394):310–320.

- Fahrmeir, L. and Kneib, T. (2009). Propriety of posteriors in structured additive regression models: Theory and empirical evidence. *Journal of Statistical Planning and Inference*, 139(3):843–859.
- Fahrmeir, L., Kneib, T., and Lang, S. (2004). Penalized structured additive regression for space-time data: a Bayesian perspective. *Statistica Sinica*, 14(3):731–761.
- Fahrmeir, L. and Lang, S. (2001). Bayesian semiparametric regression analysis of multicategorical time-space data. *Annals of the Institute of Statistical Mathematics*, 53:11–30.
- Gamerman, D. (1997). Sampling from the posterior distribution in generalized linear mixed models. *Statistics and Computing*, 7(1):57–68.
- Gelman, A. (2006). Prior distributions for variance parameters in hierarchical models. *Bayesian Analysis*, 1(3):515–534.
- Gelman, A., Carlin, J., Stern, H., and Rubin, D. (1992). Inference from iterative simulation using multiple sequences. *Statistical Science*, 7(4):457–511.
- Gelman, A. and Hill, J. (2006). *Data analysis using regression and multilevel/hierarchical models*. Cambridge University Press.
- Gelman, A., Stern, H. S., Carlin, J. B., Dunson, D. B., Vehtari, A., and Rubin, D. B. (2013). *Bayesian data analysis*. Chapman and Hall/CRC.
- Gelman, A. and Tuerlinckx, F. (2000). Type s error rates for classical and bayesian single and multiple comparison procedures. *Computational Statistics*, 15(3):373–390.
- Gilbert, B., Ogburn, E. L., and Datta, A. (2025). Consistency of common spatial estimators under spatial confounding. *Biometrika*, 112(2):asae070.
- Guan, Y., Page, G. L., Reich, B. J., Ventrucci, M., and Yang, S. (2022). A spectral adjustment for spatial confounding. *Biometrika*, 110(3):699–719.
- Hanks, E. M., Schliep, E. M., Hooten, M. B., and Hoeting, J. A. (2015). Restricted spatial regression in practice: geostatistical models, confounding, and robustness under model misspecification. *Environmetrics*, 26(4):243–254.
- Khan, K. and Calder, C. A. (2020). Restricted spatial regression methods: implications for inference. *Journal of the American Statistical Association*, 117(537):482–494.
- Klein, N., Kneib, T., et al. (2016). Scale-dependent priors for variance parameters in structured additive distributional regression. *Bayesian Analysis*, 11(4):1071–1106.
- Klein, N., Kneib, T., Lang, S., Sohn, A., et al. (2015). Bayesian structured additive distributional regression with an application to regional income inequality in germany. *The Annals of Applied Statistics*, 9(2):1024–1052.

- Mäkinen, J., Numminen, E., Niittynen, P., Luoto, M., and Vanhatalo, J. (2022). Spatial confounding in Bayesian species distribution modeling. *Ecography*, 2022(11):e06183.
- Marques, I. and Kneib, T. (2022). Discussion on ‘spatial+: A novel approach to spatial confounding’ by Dupont, E., Wood, S. and Augustin, N. *Biometrics*.
- Marques, I., Kneib, T., and Klein, N. (2022). Mitigating spatial confounding by explicitly correlating Gaussian random fields. *Environmetrics*, 33(5):e2727.
- McCandless, L. C., Gustafson, P., and Austin, P. C. (2009). Bayesian propensity score analysis for observational data. *Statistics in Medicine*, 28(1):94–112.
- Neal, R. M. (2011). Mcmc using hamiltonian dynamics. In *Handbook of Markov Chain Monte Carlo*, volume 2, page 2. CRC press.
- Nychka, D. W. (2000). Spatial-process estimates as smoothers. In Schimek, M. G., editor, *Smoothing and Regression: Approaches, Computation, and Application*. Wiley.
- Paciorek, C. J. (2010). The importance of scale for spatial-confounding bias and precision of spatial regression estimators. *Statistical Science*, 25(1):107–125.
- Ramsay, T. (2002). Spline smoothing over difficult regions. *Journal of the Royal Statistical Society Series B: Statistical Methodology*, 64(2):307–319.
- Reich, B. J., Hodges, J. S., and Zadnik, V. (2006). Effects of residual smoothing on the posterior of the fixed effects in disease-mapping models. *Biometrics*, 62(4):1197–1206.
- Reich, B. J., Yang, S., and Guan, Y. (2022). Discussion on ‘spatial+: A novel approach to spatial confounding’ by dupont, wood, and augustin. *Biometrics*, 78(4):1291–1294.
- Riebl, H., Wiemann, P. F., and Kneib, T. (2022). Liesel: a probabilistic programming framework for developing semi-parametric regression models and custom Bayesian inference algorithms. *arXiv preprint arXiv:2209.10975*.
- Sangalli, L. M., Ramsay, J. O., and Ramsay, T. O. (2013). Spatial spline regression models. *Journal of the Royal Statistical Society Series B: Statistical Methodology*, 75(4):681–703.
- Schmidt, A. M. (2022). Discussion on “spatial+: A novel approach to spatial confounding” by emiko dupont, simon n. wood, and nicole h. augustin. *Biometrics*, 78(4):1300–1304.
- Stan Development Team (2023). Stan modeling language users guide and reference manual. <https://mc-stan.org>.
- Stephens, D. A., Nobre, W. S., Moodie, E. E., and Schmidt, A. M. (2023). Causal inference under mis-specification: adjustment based on the propensity score (with discussion). *Bayesian Analysis*, 18(2):639–694.

- Thaden, H. and Kneib, T. (2018). Structural equation models for dealing with spatial confounding. *The American Statistician*, 72(3):239–252.
- Ugarte, M., Adin, A., and Goicoa, T. (2017). One-dimensional, two-dimensional, and three dimensional B-splines to specify space–time interactions in Bayesian disease mapping: model fitting and model identifiability. *Spatial Statistics*, 22:451–468.
- Urdangarin, A., Goicoa, T., Kneib, T., and Ugarte, M. D. (2024). A simplified spatial+ approach to mitigate spatial confounding in multivariate spatial areal models. *Spatial Statistics*, 59:100804.
- Urdangarin, A., Goicoa, T., and Ugarte, M. D. (2022). Evaluating recent methods to overcome spatial confounding. *Revista Matemática Complutense*, 36:333–360.
- Vehtari, A., Gelman, A., Simpson, D., Carpenter, B., and Bürkner, P.-C. (2021). Rank-normalization, folding, and localization: an improved R-hat for assessing convergence of MCMC (with discussion). *Bayesian Analysis*, 16(2):667–718.
- Wahba, G. (1984). Partial spline models for the semi-parametric estimation of several variables. In *Statistical Analysis of Time Series, Proceedings of the Japan US Joint Seminar*, pages 319–329.
- Wand, M. P. (2000). A comparison of regression spline smoothing procedures. *Computational Statistics*, 15:443–462.
- Wood, S. N. (2003). Thin plate regression splines. *Journal of the Royal Statistical Society: Series B (Statistical Methodology)*, 65(1):95–114.
- Wood, S. N. (2016). Just another Gibbs additive modeller: interfacing JAGS and mgcv. *Journal of Statistical Software*, 75(7):1–15.
- Zimmerman, D. L. and Ver Hoef, J. M. (2021). On deconfounding spatial confounding in linear models. *The American Statistician*, 76(2):159–167.